Opto-Electronic Advances

Original Article

2019, Vol. 2, No. 7

DOI: 10.29026/oea.2019.180029

Polarization multiplexing for double images display

Jinying Guo[1,2,3], Teng Wang[3], Baogang Quan[4], Huan Zhao[3], Changzhi Gu[4], Junjie Li[4], Xinke Wang[3]*, Guohai Situ[1,2]* and Yan Zhang[3]*

Metasurface provides subwavelength structures for manipulating wavefronts of light. The benefits of subwavelength components offer a continuous modulation of amplitude, phase, and polarization, thus eliminating the production of higher-order images and improving the utilization of light intensity. Despite the rapid progress in this field, multiparameter control of light using single layer metasurface is rarely reported. In fact, multiparameter control of light helps to improve information storage capacity and image fidelity. With simultaneous manipulation of polarization and amplitude at each pixel, it is possible to encode two separate images into one metasurface and reconstruct them under proper conditions. In a proof of concept experiment, we demonstrate an independent display of two binary images at the same position with polarization de-multiplexing from a single metasurface. This unique technology of encoding two images through amplitude and polarization manipulation provides a new opportunity for various applications in, such as encryption, information storage, polarization holograms, optical communications and fundamental physics.

Keywords: metasurface; multiparameter; polarization encoding

Guo J Y, Wang T, Quan B G, Zhao H, Gu C Z *et al*. Polarization multiplexing for double images display. *Opto-Electron Adv* **2**, 180029 (2019).

Introduction

Human eyes and cameras are sensitive to optical patterns with spatially varying intensity or color profiles. However, the phase and polarization states of light are usually ignored due to the inability of general optical elements to distinguish these variations. In fact, the missed phase retardation and polarization states of light usually contain abundant information[1–3]. Phase information is usually recorded and reconstructed by holography technology based on interference[4–6]. For polarization, natural light sources and materials are mostly polarized in disorganized and isotropic manners. Even under experimental circumstances, the polarization of light is commonly restricted to a single state, such as linear polarization or circular polarization. To make use of polarization information, it is necessary to generate arbitrary polarization states. Fortunately, the development of metasurfaces makes it possible to produce complex polarization states. It is very convenient to use this concept to generate vector wavefronts such as radially polarized or angularly polarized beams[7,8]. Here, we demonstrate an approach to manipulate optical patterns with spatially- and intensity-varying polarization states by virtue of metasurface.

Traditional optical elements and bulk materials encounter many limitations in the precise control of wavefronts on a submicro scale. The development of metasurfaces is expected to solve this problem and to allow arbitrary modulation of wavefronts. Metasurfaces are two-dimensional structures consisting of subwavelength antennas. The manipulation mechanism of metasurfaces is based on the horizontal dimension of the antennas rather than longitudinal thickness[9,10], which makes them ultrathin and easily fabricated. As the

[1]Shanghai Institute of Optics and Fine Mechanics, Chinese Academy of Sciences, Shanghai 201800, China; [2]Center of Materials Science and Optoelectronics Engineering, University of Chinese Academy of Sciences, Beijing 100049, China; [3]Department of Physics, Capital Normal University, Beijing Key Laboratory of Metamaterials and Devices, Key Laboratory of Terahertz Optoelectronics, Ministry of Education, and Beijing Advanced Innovation Centre for Imaging Technology, Beijing 100048, China; [4]Beijing National Laboratory for Condensed Matter Physics, Institute of Physics, Chinese Academy of Sciences, Beijing 100190, China.

*Correspondence: X K Wang, E-mail: wxk82721@163.com; G H Situ, E-mail: ghsitu@siom.ac.cn; Y Zhang, E-mail: yzhang@cnu.edu.cn

Received: 23 December 2018; Accepted: 30 January 2019; Published: 14 July 2019

nano-technology develops, it is possible to fabricate structures much smaller than wavelength, which means that the manipulation of wavefronts could be regarded as continuous even though the structural elements are discrete. This condition allows for eliminating high-order images, enlarging field of view and improving image contrast. Due to these benefits, metasurfaces are widely employed in optoelectronic devices[11–13], near-field microscopy[14,15], optical sensing[16,17], holographic[18–20] and nonlinear optics[21,22], covering microwave, terahertz, mid-infrared and visible light ranges[23–28]. During the flourishing progress of metasurfaces, multi-parameter[29–32] control of light is essential for improving information storage capacity[33,34] and image fidelity[35,36]. Almost all works mentioned above adopt composite structures to construct the metasurface, such as taking multiple particles[29,32], double layers[30] or sub-pixels[31] as a control unit. Refs. [30–32] did not involve the spatial distribution of polarization states, but focus on the response to orthogonal incidence polarization states. Grating structures were adapted by Xie et al.[37] to achieve multiparameter control. The advantage of this method is the realization of all-parameter control of light. In fact, the pixel pitch is larger than wavelength, so there are multiple levels of diffraction and the images are displayed in different places. Moreover, two sets of structures are used to control the two images. This method mentioned here is able to inhibit the production of high order images. The approach mentioned in Yue et al.'s[38] work focuses on the hiding of grayscale images with polarization manipulation. However, only one image is encoded under mutually orthogonal polarization illuminations. Here, we propose a concept to simultaneously manipulate the polarization and amplitude of light and to encode two separate images into a single metasurface. In this work, the incident polarization is fixed, and generated polarization state is spatially varied. The images are successfully recovered with polarization demultiplexing in the experiment.

Methods

The schematic of our approach to encode two images into a metasurface is shown in Fig. 1(a). A uniform plane wave with right-circular polarization passes through the designed metasurface and carries the vector property. The polarization state at each pixel becomes linear but with different directions. The images displayed without a polarizer are disorganized. Because of the spatial variation of polarization states, intensity distributions are different for the two orthogonal polarization components. If a polarizer is properly inserted in front of the detector, one target image will emerge. Another image will appear when the polarizer is rotated 90 degrees. It is noted that the image we obtained is directly behind the surface of the metasurface. For viewing purposes, the two images are staggered in the diagram, while in actuality they are in the same position. Fig. 1(b) gives out part of the metasurface in front view.

Supposing that there are two separate intensity only images $A(x, y)$ and $B(x, y)$, we can obtain the total amplitude and polarization distributions by vector superposition,

$$\boldsymbol{E}(x,y)=A(x,y)\boldsymbol{i}+B(x,y)\boldsymbol{j} \quad . \tag{1}$$

Equation (1) gives the modulation function. The reconstruction process can be realized by multiplying unit vectors independently with equation (1),

$$A(x,y)=\boldsymbol{E}(x,y)\cdot\boldsymbol{i} \quad , \tag{2}$$

$$B(x,y)=\boldsymbol{E}(x,y)\cdot\boldsymbol{j} \quad . \tag{3}$$

The polarizer can be regarded as unit vectors $\boldsymbol{i}$ or $\boldsymbol{j}$ corresponding to two orthogonal directions.

Since the designed metasurface should fit with equation (1), the intensity profile $I(x, y)$ and rotation angle $\theta(x, y)$ can be calculated as follows:

$$I(x,y)=A(x,y)^2+B(x,y)^2 \quad , \tag{4}$$

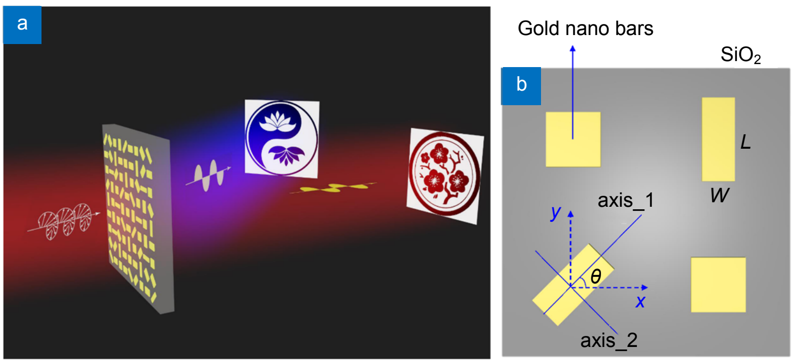

Fig. 1 | (**a**) Schematics illustrating the principle and structural design of a metasurface. A uniform planar wave with right circular polarization is irradiated on the metasurface of spatial structural changes, the emitted light field will therefore carry varying amplitude and polarization in space. Intensity distribution is different in two orthogonal polarization components, so the patterns detected at different polarization angles will be different as shown in the left graphic. For viewing purpose, two images are staggered in diagram, but in reality, they are in the same position. (**b**) Front view of part of the metasurface, the nano bars are made of gold with varied sizes and rotations, the substrate is SiO_2 with refractive index n=1.45.

$$\theta(x,y)=\arctan\{\frac{B(x,y)}{A(x,y)}\}+\frac{\pi}{4} \quad . \tag{5}$$

Because the output linear polarization for each pixel is along the angular bisector of the long and short axes of the metal bar, there is an addition of π/4 in equation (5). For simplicity, two binary images are considered to verify this idea, which means the values of A and B are 0 or 1. There are four possibilities for synthesis, (0, 0), (0, 1), (1, 0) and (1, 1), including three different total intensity values (0, 1, 2) and three different polarization directions (−π/4, 0, π/4). Simulated transmittances of nano bars in x and y polarizations under circularly polarized incident light are shown in Fig. 2, and the corresponding parameters are listed in Table 1. The total transmittance, calculated as $T=T_x+T_y=(I_x+I_y)/I_{in}$, where I_x and I_y are intensities for x and y polarized components, I_{in} is the intensity for the incident circular polarized light. For the three bars, the total transmittances are 0.01, 0.20 and 0.41, which are approximate to intensity ratio 0, 1 and 2 in the design. All parameters and results are optimized and simulated using a commercial software of FDTD solutions. The pixel pitch is 300 nm, nano bars are gold with a thickness of 30 nm, and the substrate is SiO_2 (n=1.45). Periodic boundary conditions were applied in both x and y directions, while the perfectly matched-layer boundary condition was applied in z direction. Normally incident x-polarized and y-polarized plane waves with phase delay of π/2 were used to excite the structures, and a monitor was set behind the structure to detect both x-polarized and y-polarized components of transmitted electric field. It can be seen that the simulation results meet the design requirements well.

Results and discussion

To demonstrate this idea, two binary images, one of a plum blossom (as shown in Fig. 3(a)) and one of a lotus (as shown in Fig. 3(b)), with pixel numbers of 1024×1024, are adopted in the design. A composite vector graph of a partial region is shown in Fig. 3(c) (please see Methods Section). At each pixel, the length of the arrows represents the amplitude and the direction represents the polarization direction. The metasurface is designed according to the composite vector graph. After passing through the metasurface, the uniform plane wave carries amplitude information with heterogeneous polarization distribution. To confirm its existence through the intensity profile, an

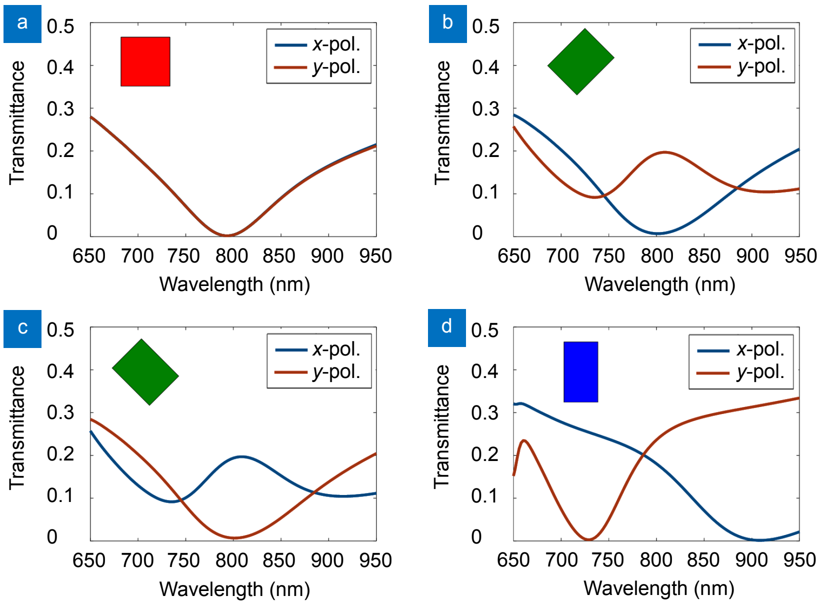

Fig. 2 | All possibilities for binary image (0, 1) synthesis. There are four cases for intensity distributions in the *x*-polarization and *y*-polarization, namely, (0, 0), (0, 1), (1, 0) and (1, 1). (**a**, **d**) show the simulated transmittance for four cases under circularly polarized incidence. Rectangles inserted in the figures represent the corresponding nano bars, which have different sizes or rotations and are optimized for 800 nm to meet the requirements. The thickness of nano bars is 30 nm, and the period is 300 nm.

Table 1 | Parameters and simulated modulation effect of three kinds of bars.

Type	Rotation angle (°)	Length (nm)	Width (nm)	Total transmittance
Red bar	0	160	160	0.01
Green bar	45	195	145	0.20
Blue bar	90	200	130	0.41

analyzer is used to extract each individual image for the x-polarized and y-polarized components. The experimental setup is shown in Fig. 4. The laser light is a linearly polarized Gaussian beam at 800 nm, and the diameter of the beam is approximately 1 cm. The light field becomes uniform and large enough to cover the whole sample after passing through the expander and collimation combination. The LP1 (polarizer) and QWP (quarter wave plate) in front of the sample are used to generate a circularly polarized beam. The output light field after the sample is imaged by a lens (magnification is about 10) and captured by a rapid CCD (charge-coupled device). The polarizer LP2 is used to extract the images by rotating the transmission axes along the horizontal or vertical directions.

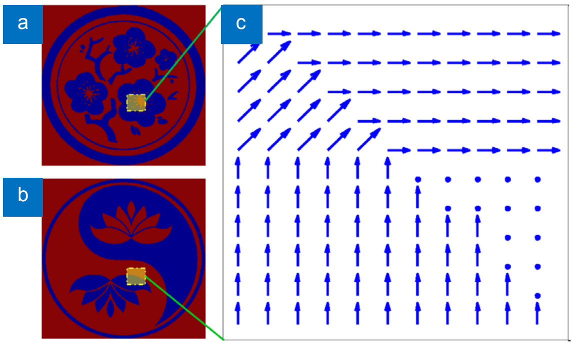

Fig. 3 | Vector composition diagram of binary images. (**a**, **b**) Binary images with pixel numbers 1024×1024 adopted in the design. (**c**) Selected vector synthesis diagram corresponding to the yellow region in (a) and (b). The dots, horizontal, vertical and slant arrows represent (0, 0), (1, 0), (0, 1) and (1, 1), respectively.

Simulated and experimental results are shown in Fig. 5. The images displayed here are corresponding to the plane of metasurface. Fig. 5(a) presents the intensity distribution captured by the CCD without the analyzer (labeled as LP2 in Fig. 4), where the intensity profile is the superposition of the two images. Fig. 5(b) shows the intensity distributions with an analyzer along the horizontal and vertical directions. The plum blossom and lotus are obviously reconstructed. The experimental results are in good agreement with expectations. There is some crosstalk in the results, which may be caused by two main factors. One is the deviation from fabrication process. Another one is the design of nanobars, which can not exactly meet the requirement, and the polarization of output light in each pixel is not purely linear. We use the sum-squared error (SSE) to describe the accuracy of the constructed image:

$$SSE = \frac{\sum (I_{\rm D} - I_{\rm FDTD})^2}{\sum I_{\rm D}^2} , \tag{6}$$

where $I_{\rm D}$ is the target image and $I_{\rm FDTD}$ is the simulated results. The SSEs for two images are 5.3e-3 and 3.6e-3, respectively, which means the images can be reconstructed well. Since the metasurface works near the resonance of nanobars, the bandwidth is quite narrow, probably 30 nm. Defects and spots appearing in both images result from fabrication errors and dusts in the CCD, which reduce the imaging clarity. To further analyze the performance of our approach, the dependence of the measured results on the direction of the transmission axis of the analyzer is shown in Fig. 5(c). The results at 0°, 30°, 45°, 60° and 90° show the evolution process of the revealed images by gradually rotating the analyzer, and the pattern gradually transforms from plum blossom to lotus. The efficiency, which is defined as the ratio of image strength with and without sample, is approximately 54%. Figure 5(d) shows the scanning electron microscope (SEM) image of the part of the metasurface. Due to manufacturing errors, the nanobars which should be rectangular became elliptical.

This experiment is for principle verification, and there is much to be improved. The nano bars can be replaced with a high refractive index dielectric to obtain higher efficiency[39-41] and the image contrast can thus be greatly improved, since the loss of dielectric is much less than metal. The discrete grayscale images can also be encoded in the metasurface by designing more nano bars. For

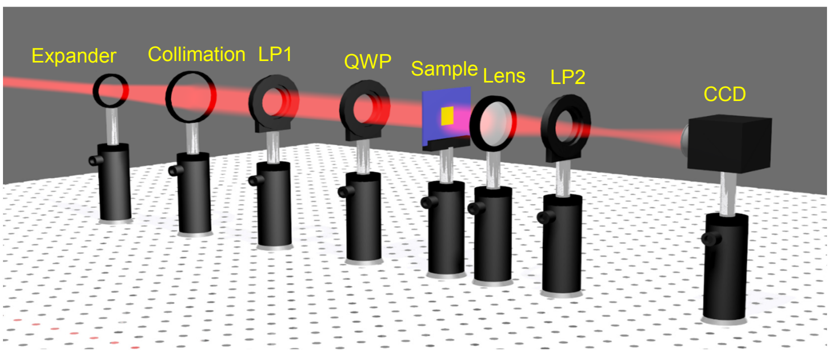

Fig. 4 | Experimental setup for polarized detection. Expander: concave lens with f= -75 mm. Collimation: convex lens with f=200 mm. LP1 and LP2: linear polarizer. QWP: quarter wave plate. Sample: designed metasurface with effective size approximately 300 μm ×300 μm. Lens: convex lens with f=50.8 mm. CCD: charge-coupled device with pixel numbers 1024×1392.

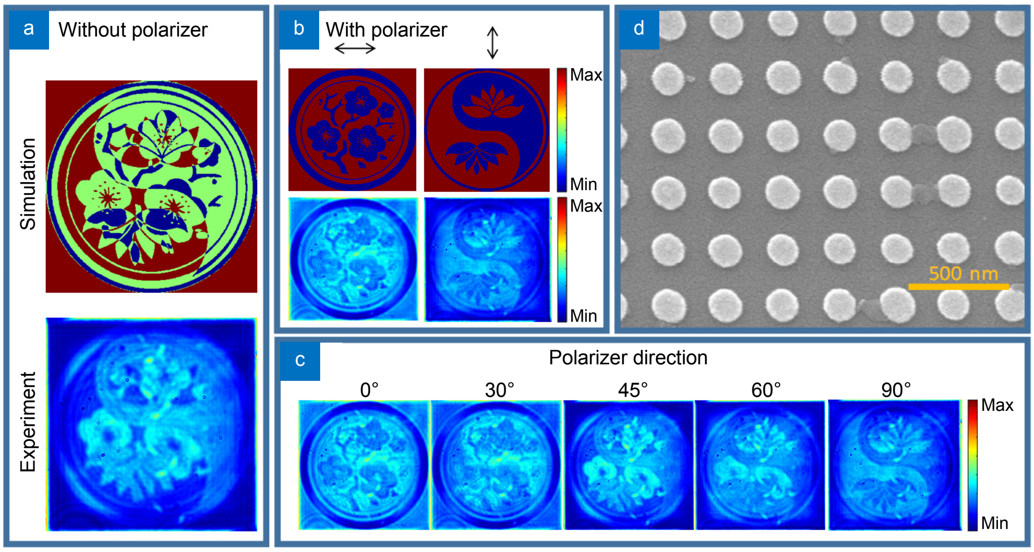

Fig. 5 | Experimental results of polarization detection. (**a**) The simulated and experimental results of images without polarizer, the intensity profile is the superposition of two images. (**b**) The simulated and experimental results of images with polarizer along the horizontal and vertical directions, respectively. (**c**) Experimental results at 0°, 30°, 45°, 60° and 90° by gradually rotating the analyzer, the pattern gradually transformed from plum blossom to lotus. (**d**) SEM image of the fabricated metasurface. The scale bar is 500 nm.

example, if two images with four levels of grayscale (0, 1, 2, 3) were to be encrypted, seven kinds of nano bars should be designed with total transmittance increasing linearly from 0 to 6. The linearly polarized light with different intensities could be generated. Then, the decomposition of light intensity into two polarization directions could be achieved by rotating the bars.

It is worth comparing the phase-polarization control[42,43] with amplitude-polarization control. Admittedly, phase modulation is more efficient than amplitude modulation. However, the design of pure phase modulation is cumbersome or unnecessary for some applications. As a complementary approach, the design of amplitude modulation is straightforward and simple. For example, the radially polarized airy beam only needs amplitude-polarization modulation, which can be easily realized with this method. Furthermore, the antennas are made of metal and the fabrication process is relatively simpler than that of dielectric metasurfaces.

Conclusions

In summary, we have demonstrated a method to modulate multiparameters of light using a metasurface. Through simultaneous manipulation of amplitude and polarization, we encoded two binary images into a single metasurface and successfully revealed the images. The proof-of-concept experimental result is in good agreement with theoretical expectations. Despite the relatively low image contrast in the experiments, this method could be improved using an all-dielectric metasurface and extending to grayscale images. This method can be applied in optical image encryption, information storage, polarization holograms, optical communications and fundamental physics.

References

1. Waller L, Tian L, Barbastathis G. Transport of intensity phase-amplitude imaging with higher order intensity derivatives. *Opt Express* **18**, 12552–12561 (2010).
2. de Boer J F, Milner T E, van Gemert M J C, Nelson J S. Two-dimensional birefringence imaging in biological tissue by polarization-sensitive optical coherence tomography. *Opt Lett* **22**, 934–936 (1997).
3. Cense B, Gao W H, Brown J M, Jones S M, Jonnal R S *et al*. Retinal imaging with polarization-sensitive optical coherence tomography and adaptive optics. *Opt Express* **17**, 21634–21651 (2009).
4. Upatnieks J, Marks J, Fedorowicz R. Color holograms for white light reconstruction. *Appl Phys Lett* **8**, 286–287 (1966).
5. Kong D Z, Shen X J, Shen Y Q, Wang X. Multi-image encryption based on interference of computer generated hologram. *Optik* **125**, 2365–2368 (2014).
6. Cuche E, Bevilacqua F, Depeursinge C. Digital holography for quantitative phase-contrast imaging. *Opt Lett* **24**, 291–293 (1999).
7. Yue F Y, Wen D D, Xin J T, Gerardot B D, Li J S *et al*. Vector vortex beam generation with a single plasmonic metasurface. *ACS Photonics* **3**, 1558–1563 (2016).
8. Liu Y C, Ling X H, Yi X N, Zhou X X, Luo H L *et al*. Realization of polarization evolution on higher-order poincaré sphere with metasurface. *Appl Phys Lett* **104**, 191110 (2014).
9. Pors A, Nielsen M G, Della Valle G, Willatzen M, Albrektsen O *et al*. Plasmonic metamaterial wave retarders in reflection by orthogonally oriented detuned electrical dipoles. *Opt Lett* **36**, 1626–1628 (2011).
10. Blanchard R, Aoust G, Genevet P, Yu N F, Kats M A *et al*. Modeling nanoscale v-shaped antennas for the design of optical

phased arrays. *Phys Rev B* **85**, 155457 (2012).
11. Fan K B, Suen J Y, Liu X Y, Padilla W J. All-dielectric metasurface absorbers for uncooled terahertz imaging. *Optica* **4**, 601–604 (2017).
12. Chen Z H, Tao J, Gu J H, Li J, Hu D *et al*. Tunable metamaterial-induced transparency with gate-controlled on-chip graphene metasurface. *Opt Express* **24**, 29216–29225 (2016).
13. High A A, Devlin R C, Dibos A, Polking M, Wild D S *et al*. Visible-frequency hyperbolic metasurface. *Nature* **522**, 192–196 (2015).
14. Arbabi E, Arbabi A, Kamali S M, Horie Y, Faraji-Dana M *et al*. MEMS-tunable dielectric metasurface lens. *Nat Commun* **9**, 812 (2018).
15. Arbabi A, Arbabi E, Kamali S M, Horie Y, Han S *et al*. Miniature optical planar camera based on a wide-angle metasurface doublet corrected for monochromatic aberrations. *Nat Commun* **7**, 13682 (2016).
16. Miyazaki H T, Kasaya T, Iwanaga M, Choi B, Sugimoto Y *et al*. Dual-band infrared metasurface thermal emitter for CO_2 sensing. *Appl Phys Lett* **105**, 121107 (2014).
17. Heydari S, Rastan I, Parvin A, Pirooj A, Zarrabi F B. Investigation of novel fractal shape of the nano-aperture as a metasurface for bio sensing application. *Phys Lett A* **381**, 140–144 (2017).
18. Wan W W, Gao J, Yang X D. Metasurface holograms for holographic imaging. *Adv Opt Mater* **5**, 1700541 (2017).
19. Ni X J, Kildishev A V, Shalaev V M. Metasurface holograms for visible light. *Nat Commun* **4**, 2807 (2013).
20. Wan W W, Gao J, Yang X D. Full-color plasmonic metasurface holograms. *ACS Nano* **10**, 10671–10680 (2016).
21. Ye W M, Zeuner F, Li X, Reineke B, He S *et al*. Spin and wavelength multiplexed nonlinear metasurface holography. *Nat Commun* **7**, 11930 (2016).
22. Walter F, Li G X, Meier C, Zhang S, Zentgraf T. Ultrathin nonlinear metasurface for optical image encoding. *Nano Lett* **17**, 3171–3175 (2017).
23. Li L L, Cui T J, Ji W, Liu S, Ding J *et al*. Electromagnetic reprogrammable coding-metasurface holograms. *Nat Commun* **8**, 197 (2017).
24. Li Y B, Li L L, Xu B B, Wu W, Wu R Y *et al*. Transmission-type 2-bit programmable metasurface for single-sensor and single-frequency microwave imaging. *Sci Rep* **6**, 23731 (2016).
25. Dong D S, Yang J, Cheng Q, Zhao J, Gao L H *et al*. Terahertz broadband low-reflection metasurface by controlling phase distributions. *Adv Opt Mater* **3**, 1405–1410 (2015).
26. Orazbayev B, Estakhri N M, Beruete M, Alù A. Terahertz carpet cloak based on a ring resonator metasurface. *Phys Rev B* **91**, 195444 (2015).
27. Yao Y, Shankar R, Kats M A, Song Y, Kong J *et al*. Electrically tunable metasurface perfect absorbers for ultrathin mid-infrared optical modulators. *Nano Lett* **14**, 6526–6532 (2014).
28. Mehmood M Q, Mei S T, Hussain S, Huang K, Siew S Y *et al*. Visible-frequency metasurface for structuring and spatially multiplexing optical vortices. *Adv Mater* **28**, 2533–2539 (2016).
29. Deng Z L, Deng J H, Zhuang X, Wang S, Li K F *et al*. Diatomic metasurface for vectorial holography. *Nano Lett* **18**, 2885–2892 (2018).
30. Almeida E, Bitton O, Prior Y. Nonlinear metamaterials for holography. *Nat Commun* **7**, 12533 (2016).
31. Wang Q, Plum E, Yang Q L, Zhang X Q, Xu Q *et al*. Reflective chiral meta-holography: multiplexing holograms for circularly polarized waves. *Light: Sci Appl* **7**, 25 (2018).
32. Zhang F, Pu M B, Li X, Gao P, Ma X L *et al*. All-dielectric metasurfaces for simultaneous giant circular asymmetric transmission and wavefront shaping based on asymmetric photonic spin-orbit interactions. *Adv Funct Mater* **27**, 1204295 (2017).
33. Li X P, Cao Y Y, Gu M. Superresolution-focal-volume induced 3.0 Tbytes/disk capacity by focusing a radially polarized beam. *Opt Lett* **36**, 2510–2512 (2011).
34. Gao H, Rosenberry M, Batelaan H. Light storage with light of arbitrary polarization. *Phys Rev A* **67**, 053807 (2003).
35. Rong L, Xiao W, Pan F, Liu S, Li R. Speckle noise reduction in digital holography by use of multiple polarization holograms. *Chin Opt Lett* **8**, 653–655 (2010).
36. Yuan C J, Situ G H, Pedrini G, Ma J, Osten W. Resolution improvement in digital holography by angular and polarization multiplexing. *Appl Opt* **50**, B6–B11 (2011).
37. Xie Z W, Lei T, Si G Y, Wang X Y, Lin J *et al*. Meta-holograms with full parameter control of wavefront over a 1000 nm bandwidth. *ACS Photonics* **4**, 2158–2164 (2017).
38. Yue F Y, Zhang C M, Zang X F, Wen D D, Gerardot B D *et al*. High-resolution grayscale image hidden in a laser beam. *Light: Sci Appl* **7**, 17129 (2018).
39. Decker M, Staude I, Falkner M, Dominguez J, Neshev D N *et al*. High-efficiency dielectric huygens' surfaces. *Adv Opt Mater* **3**, 813–820 (2015).
40. Devlin R C, Khorasaninejad M, Chen W T, Oh J, Capasso F. Broadband high-efficiency dielectric metasurfaces for the visible spectrum. *Proc Natl Acad Sci USA* **113**, 10473–10478 (2016).
41. Arbabi E, Arbabi A, Kamali S M, Horie Y, Faraon A. High efficiency double-wavelength dielectric metasurface lenses with dichroic birefringent meta-atoms. *Opt Express* **24**, 18468–18477 (2016).
42. Arbabi A, Horie Y, Bagheri M, Faraon A. Dielectric metasurfaces for complete control of phase and polarization with subwavelength spatial resolution and high transmission. *Nat Nanotechnol* **10**, 937–943 (2015).
43. Mueller J P B, Rubin N A, Devlin R C, Groever B, Capasso F. Metasurface polarization optics: independent phase control of arbitrary orthogonal states of polarization. *Phys Rev Lett* **118**, 113901 (2017).

Acknowledgements

This work was supported by the 973 Program of China (grant No. 2013CBA01702); the National Natural Science Foundation of China (grant Nos. 11474206, 11404224, 1174243, and 11774246); the Beijing Youth Top-Notch Talent Training Plan (CIT&TCD 201504080); the Beijing Nova Program (grant No. Z161100004916100); the Beijing Talents Project (grant No. 2018A19); Capacity Building for Science & Technology Innovation-Fundamental Scientific Research Funds (grand No. 025185305000/142) and the Scientific Research Base Development Program of the Beijing Municipal Commission of Education.

Competing interests

The authors declare no competing financial interests.